Chemical Physics 127 (1988) 297–304
North-Holland, Amsterdam

AN OPTICALLY DETECTED MAGNETIC RESONANCE STUDY OF Mn^{4+} IN Cs_2GeF_6 AND K_2GeF_6

E. LIFSHITZ and A.H. FRANCIS

Department of Chemistry, University of Michigan, Ann Arbor, MI 48109-1055, USA

Received 4 April 1988

The photoexcitation and photoluminescence spectra ($^2E \leftrightarrow {}^4A_2$) of MnF_6^{2-} diluted in Cs_2GeF_6 and K_2GeF_6 host lattices have been recorded at liquid helium temperature. The manganese coordination geometry is O_h in Cs_2GeF_6 and D_{3d} in K_2GeF_6. Optically detected magnetic resonance (ODMR) has been employed to determine the g value of the ^2E state in both coordination geometries. The trigonal distortion has a pronounced effect on the g value and produces a measurable splitting in the optical spectrum, but exerts relatively little effect on the radiative lifetime. The g value in the O_h site ($g(^2E) = 2.0$) is as predicted theoretically; however, the value obtained for the D_{3d} site is unexpectedly large ($g(^2\bar{E}) = 2.95$). The data obtained are compared with theoretical predictions and the results of similar studies of d^3 ions in a variety of lattices. The differences are shown to arise, in part, from the relative magnitude of the spin–orbit coupling and the trigonal field splitting.

1. Introduction

The electronic absorption and luminescence spectra of first row transition metal ions with a d^3 configuration have been the subject of many investigations [1]. The most frequently studied d^3 ion is certainly Cr^{3+}, but the isoelectronic ions of V^{2+} and Mn^{4+} have also been extensively examined. All three of these ions have been investigated by Geschwind and co-workers [2,3] as substitutional impurity centers in corundum (Al_2O_3). This very detailed comparative study illustrated the influence of the strong trigonal distortion present in the corundum lattice. In addition to breaking the four-fold degeneracy of the ^2E state, the distortion (in combination with spin–orbit coupling) strongly affects the excited state g value, the radiative lifetime and the spin relaxation time, T_1.

Exceptionally well resolved and highly structured absorption and luminescence spectra have been previously obtained from Mn^{4+} in alkali metal (A) hexafluorogermanates (A_2GeF_6). As a result, the spectra obtained from these host lattices have been studied by numerous researchers and are now analyzed in considerable detail. Most band positions and splittings are accurately recorded and many of the observed features have been convincingly assigned to the predicted crystal field transitions of a d^3 ion. Only a few details of the spectra remain unresolved and these involve the location of the doublet states and the proper assignment of the spin–orbit components of the quartet states.

The A_2GeF_6 lattices offer a significant advantage over the corundum lattice for the study of crystal field effects on the excited state magnetic properties of Mn^{4+}. Mn^{4+} may be introduced substitutionally for germanium without charge compensation; Mn^{4+} cannot substitute directly for Al^{3+} in the corundum lattice without charge compensation. This was provided by the introduction of Mg^{2+} ions in earlier studies [3], which complicates the interpretation of the crystal field site symmetry.

This paper presents the results of a study of Mn^{4+} substitutional impurity centers in Cs_2GeF_6 and K_2GeF_6. Based on the crystal structures of the host lattices, the manganese coordination is expected to be octahedral in Cs_2GeF_6 [4] and is trigonally distorted D_{3d} in K_2GeF_6 [5]. Comparison of the results from the two lattices provides an

opportunity to examine the effects of the trigonal field on the magnetic and dielectric parameters of the excited $^2E(t_2^3)$ state.

2. Experimental

2.1. Sample preparation

The crystals used in the present study contained approximately 3–6% Mn^{4+} and were obtained as single crystal platelets approximately $3 \times 3 \times 1$ mm^3 by slow evaporation of solutions containing the mixed salts in 40% HF solution. Details of the procedure have been described previously [6].

2.2. Photoexcitation and photoluminescence spectra

Photoexcitation spectra were obtained with the sample crystals cooled to approximately 5 K by the vapor from normal boiling liquid helium. Luminescence was excited by the output from a 1 kW Osram xenon arc lamp, monochromated by a 1/4 m scanning monochromator. The excitation monochromator bandpass was 1 Å. Photoexcitation spectra were recorded by monitoring the total sample luminescence intensity with an RCA 4840 photomultiplier.

Luminescence spectra were recorded with an ITT scanning monochromator equipped with an RCA C31041 photomultiplier. The spectra were obtained with a bandpass of 1 Å and were calibrated with the output of an iron–neon hollow cathode lamp.

Radiative lifetime measurements were performed by pulse excitation of the sample using a nanosecond duration, atmospheric pressure pulsed arc. The luminescence decay was averaged using a Tracor–Northern NS-575 signal averager.

2.3. ODMR of the ^2E state

The ODMR technique applied to the excited states of transition metal ions in inorganic lattices has been discussed in detail previously [7]. The experimental apparatus for ODMR measurements was generally similar to that described by Imbusch et al. [3], but differed in several details. In particular, a small, X-band, TE_{011} cyclindrical microwave cavity with an unloaded Q of approximately 3000 was used. A hole was bored concentric with the cavity axis, and two at right angles to the axis, to permit insertion of the sample, irradiation of the sample and collection of luminescence.

Up to 2 W of microwave power at a frequency of 10.861 GHz was provided by the combination of a Hewlett–Packard 8690B sweeper and and TWT power amplifier. The microwave power was coupled to the cavity with a small loop formed at the end of a three foot length of semirigid coaxial cable. The cavity was located concentrically within the bore of a superconducting solenoid. The magnet coils could produce a maximum field of about 2 T with a field homogeneity over the sample volume of about 10^{-4}. The field was calibrated by detecting the cavity loss at resonance with a sample of DPPH.

The magnet and the cavity were immersed in superfluid liquid helium at about 2 K. Sample crystals were afixed to a quartz fiber support rod and suspended within the cylindrical microwave cavity. Luminescence was excited using the 4580 Å output of an Ar^+ laser. The ODMR signal was demodulated by a lock-in amplifier referenced to the amplitude modulation frequency of the microwave generator.

3. Results

3.1. Photoexcitation and luminescence spectra

The low temperature (4 K) absorption spectra of MnF_6^{2-} in both Cs_2GeF_6 and K_2GeF_6 lattices have been recorded and analyzed in detail by Helmholtz and Russo [6]. The photoexcitation spectra have not been studied previously at 4 K, however, Paulusz [8] examined the excitation spectra of Mn^{4+} in a variety of hexafluoride lattices at 90 K.

The photoexcitation spectra of MnF_6^{2-} in Cs_2GeF_6 and K_2GeF_6, obtained at approximately 4 K, consist of three widely separated band systems. The spectrum of MnF_6^{2-} in the Cs_2GeF_6

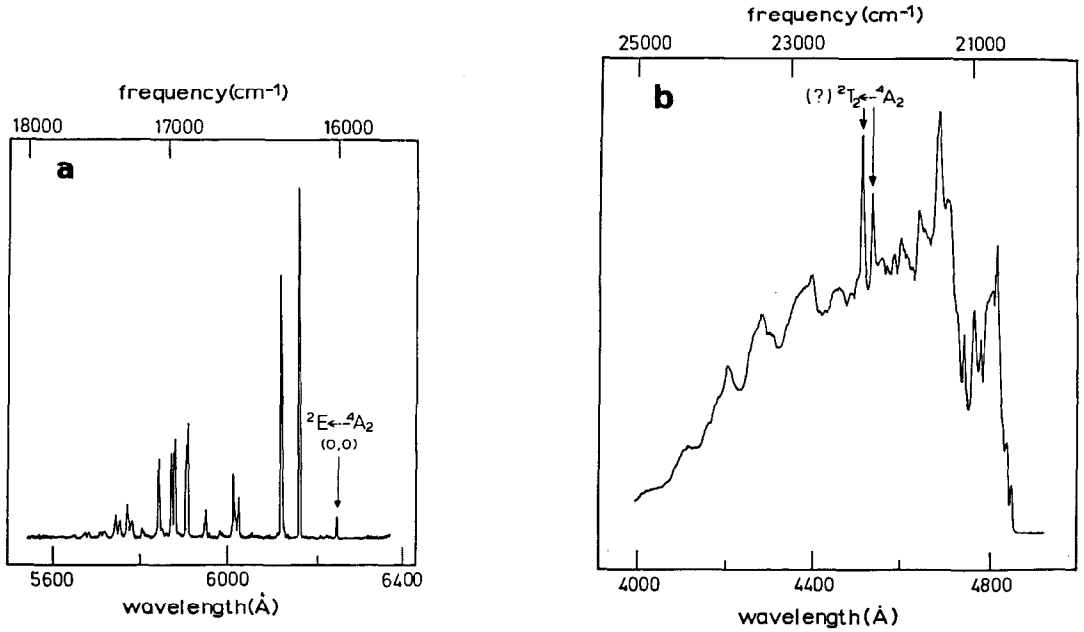

Fig. 1. (a) and (b). The photoexcitation spectrum of Cs_2GeF_6 recorded at 5 K.

host lattice is reproduced in figs. 1a and 1b. Only the positions of the electronic and vibronic origin bands are reported in table 1 and these were found to be in close agreement with the values reported by previous workers [6,8,9]. The photoexcitation spectrum of MnF_6^{2-} in K_2GeF_6 shows additional splittings due to the small trigonal distortion of the octahedral coordination but is otherwise similar to the spectrum in Cs_2GeF_6 and is not reproduced here.

Several differences are apparent when the photoexcitation spectra are compared with the absorption spectra. Some intense features of the excitation spectrum evidently correspond to relatively weak bands of the absorption spectrum; some features of the absorption spectrum have no counterparts in the excitation spectrum. In particular, two prominent excitation bands near 4550 Å are weak or absent in the absorption spectrum. These bands (annotated in fig. 1b) may correspond to the transition $^2T_2 \leftarrow {}^4A_2$. This transition has previously been assigned, tentatively, to a higher energy band system, described as a very weak shoulder, at 25707 cm^{-1} [10]. The transition may be enhanced in the excitation spectrum due to the high rate of radiationless relaxation $^2T_2 \rightarrow {}^2E$. The sharpness of the prominent band system is consistent with a transition to a nearly *Dq* independent state.

Additionally, the $(^4P, e^2t_2^1)$ $^4T_2 \leftarrow {}^4A_2$ band near 2400 Å is prominent in absorption but absent in the photoexcitation spectrum. The differences between the absorption and excitation spectra are all plausibly associated with differences in the non-radiative relaxation pathways from the several excited electronic states observed. Although the photoexcitation spectra provide a few additional

Table 1
Band positions and assignments in several host lattices

Lattice	^2E	$^2T_1$	$^4T_2$	$^2T_2$	$^4T_1$
Cs_2GeF_6 [a]	16032	16706 16788	20630	22000	26000
K_2GeF_6 [a]	16070 16081	16800	20550	22000	–
$Al_2O_3(Mg)$ [b]	14782	15500	20800	21200	25000
Cs_2MnF_6 [c]	16071	17300	21801	25707	28530

[a] Ref. [6] and present work.
[b] Ref. [3] [c] Ref. [10].

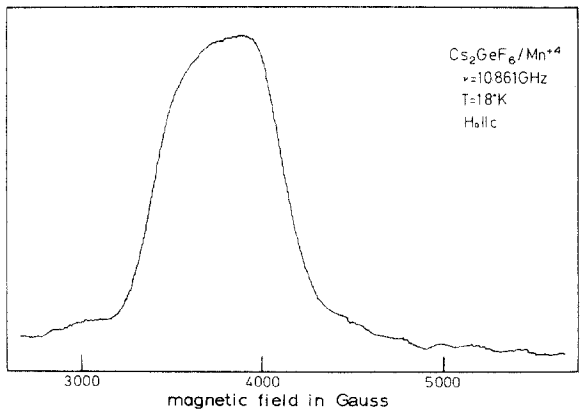

Fig. 2. The ODMR spectrum of the Mn^{4+} ^2E state in Cs_2GeF_6.

insights into state assignments, their importance in the present work is to establish the correspondence between our samples and those previously studied.

3.2. ODMR spectra

The ODMR observations of the ^2E excited state were carried out by monitoring the intensity change in the circularly polarized light emitted from this level along the direction of the external magnetic field as the field was swept through resonance. A representative ODMR spectrum obtained for Mn^{4+} in Cs_2GeF_6 is illustrated in fig. 2. The resonance line, centered at 3.9 kG ($g = 1.99$), is approximately 750 G wide (fwhm) and probably consists of unresolved manganese ($I_{nuc} = 5/2$) nuclear hyperfine structure. The ODMR spectrum of MnF_6^{2-} in K_2GeF_6 exhibits a resonance peak at 2.6 kG ($g = 2.97$), approximately 1000 G wide (fwhm) (fig. 3).

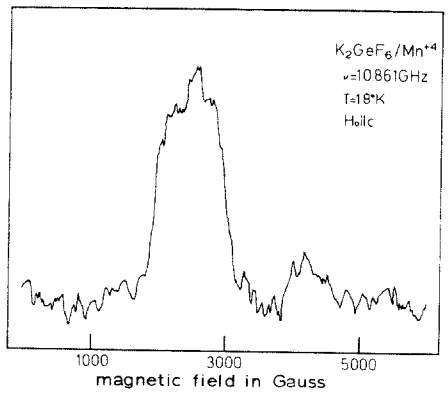

Fig. 3. The ODMR spectrum of the Mn^{4+} ^2E state in K_2GeF_6.

4. Discussion

The ^4F free-ion ground state of $Mn^{4+}(3d^3)$ is split in an octahedral field into a $^4A_2(t_2^3)$ ground state and $^4T_2(e^1t_2^2)$ and $^4T_1(e^1t_2^2)$ electronic excited states. In crystal fields of moderate strength, the lowest-lying electronic excited state is the $^2E(t_2^3)$ level derived from the free-ion ^2G state. The $^2T_1(t_2^3)$ and $^2T_2(t_2^3)$ states, also derived from the free-ion ^2G term, are important in the interpretation of the spectra.

In octahedral coordination, the ^2E state is two-fold spin degenerate and two-fold orbital degenerate. Neither spin–orbit coupling nor an external magnetic field removes the two-fold orbital degeneracy. This is the situation expected for Mn^{4+} as a substitutional impurity in Cs_2GeF_6 where it replaces octahedrally coordinated Ge. K_2GeF_6 belongs to the space group D_{3d}^3 [5] and the manganese coordination is expected to be trigonally distorted. The distortion results in an axial splitting of the ground state $^4A_2$ of 0.7 cm^{-1} and a 10 cm^{-1} splitting of the ^2E state [6]. A partial energy level diagram (fig. 4) illustrates the splitting of the ground state and first excited state in a trigonal crystal field and an external magnetic field.

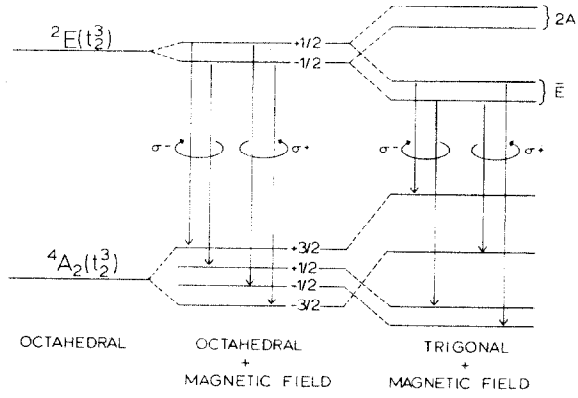

Fig. 4. Octahedral and trigonal crystal field levels in ^2E in an external magnetic field. The optical transitions detected for ODMR measurements are illustrated.

Table 2
Collected spectroscopic parameters for d^3 ions

Lattice/ion	$\lambda(^2E)$ (cm^{-1})	$\delta(^4A)$ (cm^{-1})	$\lvert g_{\parallel}\rvert$	t_R (ms)	K (cm^{-1})	ζ (cm^{-1})	$\zeta^{0\,a)}$ (cm^{-1})
Al_2O_3/Mn^{4+} b)	81	0.39	3.10	0.83	−450	230	410
Al_2O_3/Cr^{3+} b)	30	0.38	2.45	3.5	−350	140	270
Al_2O_3/V^{2+} b)	12.3	0.33	2.22	65	−175	100	168
K_2GeF_6/Mn^{4+}	11	0.7	2.97	14.2	−100	230	410
Cs_2GeF_6/Mn^{4+}	0	0	2.0	15.5	−100	230	410
MgO/Cr^{3+} c)	0	0	2.00				

a) Free-ion spin–orbit coupling constant.
b) Refs. [2,3]. c) Ref. [13].

4.1. The ODMR determination of excited state g values

ODMR determination of the excited state g value may be understood by reference to fig. 4. For equal population of the $+1/2$ and $-1/2$ Zeeman levels of the ^2E (or $^2\bar{E}$) state, equal intensity of left- and right-hand circularly polarized emission is emitted along the direction of the external magnetic field. At sufficiently low temperatures, the population of these states (assuming a Boltzmann distribution) becomes unequal. Then, ODMR state can be detected by monitoring the change in left or right circularly polarized phosphorescence along the direction of the magnetic field as the field is passed through resonance.

4.2. g value of the ^2E state in octhadral sites

The magnetic properties of the ^2E state can be conveniently described with the effective Hamiltonian used by Tanabe and Kamimura [11], in which irreducible tensor operators represent the non-cubic field interactions. This Hamiltonian identifies the various contributions to the g values from the trigonal distortion (V_{trig}) and spin–orbit coupling (V_{SO}). The notation employed is that used in ref. [11],

$$H_{eff} = S \cdot \lambda \cdot T(A_2) + \beta H \cdot g \cdot S + \beta H \cdot g_0 \cdot T(A_2) + \beta H \cdot g_E \cdot V(E) \cdot S. \quad (1)$$

$V(E)$ and $T(A_2)$ are tensor operators transforming as the E and A_2 irreducible representations of C_{3v}. Orbital operators of the type $T(A_2)$ give rise to non-vanishing matrix elements of orbital angular momentum (L) in combination with the external field (H) and to matrix elements of the products $L_x \times V_{trig} \times V_{trig}$ and $S_z \times V_{trig} \times V_{SO}$. Since the angular momentum is effectively quenched in the ^2E state [11,12], the third term of eq. (1) is negligible and is not considered further. Operators of the $V(E)$ type are associated with V_{SO}. For octahedral site symmetry the effective Hamiltonian is further simplified. With the external field parallel to z we obtain

$$H_{eff} = \beta H \cdot g_{\parallel} \cdot S_z + \beta H \cdot g_{E\parallel} \cdot V(E) \cdot S_z. \quad (2)$$

The effective g value is $g_{\parallel}(^2E) = g_{\parallel} + g_{E\parallel}$. Within the t_2^3 manifold of states, the ^2E state is mixed by spin–orbit coupling with only the $^2T_2$ state. We have computed the second-order correction to $g_{\parallel}(^2E)$ using matrix elements of the spin–orbit coupling and the dipole moment operator given by Eisenstein [13],

$$g_{E\parallel} = \zeta^2 / \left[W(^2E) - W(^2T_2) \right]^2. \quad (3)$$

ζ is the molecular one-electron spin–orbit coupling parameter. If the value of $\zeta = 230$ cm^{-1} [3,6,10] is adopted, eq. (3) yields $\lvert g_{E\parallel}\rvert \approx 0.001$. Spin–orbit coupling to the $^4T_2(t_2^2e^1)$ state contributes a term of similar magnitude. Therefore, in the absence of a trigonal distortion, $g_{\parallel}(^2E)$ is expected to be close to the free-electron value, as found experimentally by Sugano et al. [14] for Cr^{3+} in cubic MgO (see table 2). We find the

Mn^{4+} resonance in Cs_2GeF_6 to be centered at $g = 2.00 \pm 0.05$, also in agreement with the prediction of theory. This value supports the assumption employed in the analyses of the absorption and excitation spectra [6] that the manganese coordination in the Cs_2GeF_6 lattice is closely octahedral.

4.3. g value of the ^2E state in trigonal sites

In the presence of a trigonal distortion, eq. (1) has the following eigenvalues [11]:

$$W_{\pm}(2A) = \tfrac{1}{2}\lambda \pm \beta H\left(\tfrac{1}{2}g_{\|} + g_{0\|} + \tfrac{1}{2}g_{E\|}\right),$$
$$W_{\pm}(\bar{E}) = \tfrac{1}{2}\lambda \pm \beta H\left(\tfrac{1}{2}g_{\|} - g_{0\|} + \tfrac{1}{2}g_{E\|}\right). \quad (4)$$

The first term arises from the trigonal distortion in combination with spin–orbit coupling. Therefore, the ^2E state is split by the combined effect of these interactions into two Kramers doublets: a ^{2}2A and a $^2\bar{E}$ state separated by λ. Each doublet exhibits a linear Zeeman effect with the effective g value given by

$$g_{\|}(2A) = +g_{\|} + 2g_{0\|} + g_{E\|},$$
$$g_{\|}(\bar{E}) = -g_{\|} + 2g_{0\|} + g_{E\|}. \quad (5)$$

The trigonal splitting and g value may be expressed in terms of a small number of empirical parameters. The ^2E splitting is [11,12]

$$\lambda = 4K\zeta/\left[W(^2E) - W(^2T_2)\right], \quad (6)$$

where K is the trigonal field strength parameter. Using the parameter values and state energies from table 2, we obtain $K = -71$ for Mn^{4+} in K_2GeF_6. Since the observed g value (see below) suggests that the $^2\bar{E}$ state lies below the ^{2}2A state, $\lambda > 0$ and K is negative.

The second-order correction to the g value arising solely from matrix elements of the trigonal field is given by

$$g_{0\|} = -12K^2/\left[W(^2E) - W(^2T_2)\right] \times \left[W(^2E) - W(^2T_1)\right] - 6K^2/\left[W(^2E) - W(^2T_2)\right]^2. \quad (7)$$

With $K = -71$ cm^{-1} and the state energies from table 2, eq. (7) yields $g_{0\|} = -0.015$. A second-order correction due to matrix elements of $V_{SO} \times V_{trig}$ is also found:

$$g_{E\|} = -8\zeta K/\left[W(^2E) - W(^2T_2)\right] \times \left[W(^2E) - W(^2T_1)\right], \quad (8)$$

which yields a contribution of $g_{E\|} = -0.03$. Therefore, the computed g values for the $\bar{E}$ and 2A components of the ^2E state are $g_{\|}(2A) = 1.94$ and $g_{\|}(\bar{E}) = -2.06$.

The ODMR spectrum obtained in K_2GeF_6 is shown in fig. 3. The g value for H parallel to C_3 is determined to be 2.96, substantially larger than predicted. This result is unexpected, in view of the agreement obtained by Imbusch et al. [3] for Mn^{4+} in Al_2O_3 with $\zeta = 230$ cm^{-1} and $K = -450$ cm^{-1} (see table 2). It should be noted that the magnitude of the g value in Al_2O_3 is a result of the particular circumstance that $K > \zeta$.

We discuss briefly two possible reasons for the wide disparity between the experimental and theoretical values of $g_{\|}(\bar{E})$. Both the value of the spin–orbit coupling parameter and the energy difference $W(^2T_1) - W(^2E)$ can strongly affect the magnitude of $g_{\|}(\bar{E})$. An order of magnitude reduction in either of these quantities is required to bring the experimental and calculated values of $g_{\|}(\bar{E})$ into reasonable agreement.

The energy difference $W(^2T_1) - W(^2E)$ had been estimated variously to be 400–1200 cm^{-1} [6,10,14], but, until recently, no experimental evidence was available to suggest an accurate value. Low [15] had calculated the $^2T_1$–^2E splitting to be 400 cm^{-1} for the Cr^{3+} in MgO. Although the excitation spectrum was carefully examined in the region of the $^2T_1 \leftarrow {}^4A_2$ transition (fig. 1a), no bands were observed that could be unambiguously assigned to this transition. Recently, the spectrum of Mn^{4+} in Cs_2GeF_6 was observed by means of two-photon spectroscopy, allowing direct observation of the electronic origins of both the ^2E_g and $^2T_{1g}$ states [16]. The $W(^2T_1) - W(^2E)$ separation was found to be 705 cm^{-1}, within the range estimated by Helmholtz and Russo [6] and too large to account for the deviation of $g_{\|}(\bar{E})$.

A second parameter value that is poorly established from experiment is the magnitude of the

spin–orbit coupling interaction. The free-ion value is 410 cm^{-1}, and reduction to about half this value in the coordinated ion has been considered reasonable. A substantially greater reduction would bring the theoretical and experimental g values into closer agreement since the trigonal splitting depends on the product, $K \times \zeta$. The radiative lifetime of the excited state is inversely proportional to ζ^2, and so may be used to estimate the magnitude of this parameter in different lattices. The radiative lifetime in K_2GeF_6 is about twenty times greater than in Al_2O_3. This result suggests a reduction of ζ in K_2GeF_6 to 52 cm^{-1}. This represents a very large decrease in the free-ion spin–orbit coupling. However, if this value is used in the calculations, we obtain $K = -313$ and $g_{\|}(^2\bar{E}) = -2.61$.

4.4. $^4A_2$ ground state trigonal field splitting

Although the trigonal field splitting of the ^2E state of Mn^{4+} in K_2GeF_6 is smaller than that of Mn^{4+} in Al_2O_3, the ground state splitting is substantially larger. The ground state trigonal splitting has been obtained by Meijer and Gerritsen [17] as

$$\delta = \tfrac{4}{3}\zeta^2 K / \left[W(^4A_2) - W(^4T_2) \right]^2, \qquad (9)$$

with the assumption of isotropic spin–orbit coupling interactions. This expression leads to the incorrect sign for δ. Sugano and Tanabe [12] obtained a relationship between δ and K taking into account the effect of anisotropic spin–orbit coupling. Unfortunately, no experimental information is available with which to estimate the anisotropy.

4.5. Spin–lattice relaxation time, T_1

In addition to its effect upon the g value of the ^2E state, the trigonal field splitting is expected to influence the spin–lattice relaxation (SLR) rate. At liquid helium temperatures, SLR in the ^2E state occurs via the direct process mechanism. However, in the trigonal site of K_2GeF_6, an Orbach process is possible between the $^2 2A$ and $^2\bar{E}$ components of the ^2E state. The contribution to the SLR time (T_1) for the Orbach process is given by

$$T_1 \propto \exp(-\lambda/kT). \qquad (10)$$

In order to observe the effect of the trigonal field upon the SLR, we used the technique employed by Imbusch et al. [3]. The decay of the ODMR signal was observed subsequent to saturating the spin transition. When the saturating microwave power was switched off, the ODMR signal decayed with an exponential lifetime of approximately 16 ms. Because the spin relaxation is associated with an electronically excited state, the radiative lifetime of the state (t_R) contributes to the observed decay time (t) of the ODMR signal. The decay time is given by

$$1/t = 1/t_R + 1/T_1. \qquad (11)$$

The radiative lifetime thus imposes a limit on the longest spin–lattice relaxation time that can be measured. In both the K_2GeF_6 and Cs_2GeF_6 lattices, the decay time of the ODMR signal was within experimental error of the radiative decay time. Therefore, we may conclude that a $T \approx 2$ K, $T_1 \gg t_R$ for both lattice and is unaffected by the trigonal distortion.

Acknowledgement

The author would like to thank Dr. N. Nagasundaram for his technical assistance in the experimental measurements.

References

[1] A.B.P. Lever, Inorganic electronic spectroscopy (Elsevier, Amsterdam, 1984).
[2] S. Geschwind, G.E. Devlin, R.L. Cohen and S.R. Chinn, Phys. Rev. A 137 (1965) 1087.
[3] C.F. Imbusch, S.R. Chinn and S. Geschwind, Phys. Rev. 161 (1967) 295.
[4] R. Wyckoff, Crystal structures, Vol. 3, 2nd Ed. (Wiley, New York, 1965).
[5] W.B. Vincent and J.L. Hoard, J. Am. Chem. Soc. 64 (1942) 1233.
[6] L. Helmholtz and M.E. Russo, J. Chem. Phys. 59 (1973) 5455.
[7] R. Bernheim, Optical pumping: an introduction (Benjamin, New York, 1965).
[8] A.G. Paulusz, J. Electrochem. Soc. 120 (1973) 942.
[9] S.L. Chodos, A.M. Black and C.D. Flint, J. Chem. Phys. 65 (1976) 4816; Chem. Phys. Letters 33 (1975) 344.

[10] M.J. Reisfeld, N.A. Matwiyof and L.B. Asprey, J. Mol. Spectry. 39 (1971) 8.
[11] Y. Tanabe and H. Kamimura, J. Phys. Soc. Japan 13 (1958) 394.
[12] S. Sugano and Y. Tanabe, J. Phys. Soc. Japan 13 (1958) 394.
[13] J.C. Eisenstein, J. Chem. Phys. 34 (1961) 1628.
[14] S. Sugano, A.L. Schawlow and F. Varsanyi, Phys. Rev. 120 (1960) 2045.
[15] W. Low, J. Chem. Phys. 33 (1960) 1162.
[16] R.-L. Chien, J.M. Berg and D.S. McClure, J. Chem. Phys. 84 (1986) 4168.
[17] P.H.E. Meijer and H.J. Gerritsen, Phys. Rev. 100 (1955) 742.